Measurement-Based Dynamic Load Modeling Using the Vector Fitting Technique

Eleftherios O. Kontis, *Student Member, IEEE,* Theofilos A. Papadopoulos, *Member, IEEE,* Andreas I. Chrysochos, *Member, IEEE,* and Grigoris K. Papagiannis, *Senior Member, IEEE*

***Abstract*—Accurate load modeling is essential for power system stability analysis and control. This topic has regained interest, due to the high penetration of new types of loads and the increased availability of measurements in extended power grids. In this paper, an aggregated load model based on measurement data is formulated for dynamic simulations of large power systems. The proposed model employs variable-order transfer functions, enabling the accurate simulation of complex load dynamics. A complete methodology for the automatic derivation of the minimum-required model order is proposed with the model parameters calculated via a robust multi-signal identification procedure. For this purpose, the Vector Fitting method is introduced as a technique for measurement-based load modeling. Several simulations are performed using the NEPLAN software to investigate the accuracy and the generalization capabilities of the proposed model. The model performance is thoroughly compared with other conventional load models, using also measurements recorded on a laboratory-scale microgrid.**

***Index Terms*—Dynamic equivalencing, dynamic load modeling, measurement-based approach, multi-signal analysis, Vector Fitting.**

I. Introduction

THE interest in load modeling has been originally motivated by the fact that load characteristics have significant impact on power system dynamics, influencing considerably the angular and voltage stability limits, the inter-area oscillations and the dominant system modes [1], [2]. Recently, the interest in load modeling has been renewed due to the advent of highly efficient, low-inertia motors and mainly due to the emergence of new, non-conventional types of loads, such as air conditioners and power electronics loads [3], [4].

Despite the ongoing research efforts, the modeling of power system loads still remains one of the most uncertain areas in large-scale simulations [5]. The vast number of individual devices, constituting power system loads, as well as their stochastic and time-varying behavior, pose several difficulties and challenges in the already complex modeling procedure [6], [7]. To overcome these issues, load aggregation techniques are often employed [8].

Manuscript received July 20, 2016; revised November 25, 2016 and February 28, 2017.

E. O. Kontis, A. I. Chrysochos, and G. K. Papagiannis are with the Power Systems Laboratory, School of Electrical and Computer Engineering, Aristotle University of Thessaloniki, Thessaloniki, Greece, GR 54124, (e-mail: kontislefteris@gmail.com; anchryso@auth.gr; grigoris@eng.auth.gr).

T. A. Papadopoulos and A. I. Chrysochos are with the Power Systems Laboratory, Dept. of Electrical and Computer Engineering, Democritus University of Thrace, Xanthi, Greece, GR 67100, (e-mail: thpapad@ee.duth.gr).

Andreas I. Chrysochos is also with the Cablel® Hellenic Cables S.A., Viohalco Group, Sousaki Korinthias, Korinthos, Greece, GR 20100 (e-mail: achrysochos@fulgor.vionet.gr).

In principle, two different methodologies can be used to develop a load model, namely the component- and the measurement-based approach [8]. The former requires the *a priori* knowledge of load components and characteristics. Thus, the development of the corresponding models requires highly reliable data, which are usually difficult, if not impossible, to be determined [4], [9]. On the other hand, the measurement-based approach uses field data, obtained at the load bus, for which the load model is developed. The unknown load model parameters are typically estimated using system identification techniques [6]. The significant advantage of this approach lies in its inherent ability to directly reflect the load dynamics. This approach can also be favored in smart grids, since phasor measurement units (PMUs) can provide the required measurements almost in real-time. Whenever new measurements are available, the model parameters can be updated, enhancing gradually the robustness of the developed load model [10].

In the literature, several methods have been proposed to develop load models using the measurement-based approach. Traditionally, the majority of these methods consider a standard load model structure [1], [2] and estimate the corresponding model parameters using an optimization technique [4]. Among other optimization techniques, the nonlinear least square (NLS) method [11], [12] gradient-based techniques [13], weighted NLS methods [7], [14], adaptive-simulated annealing [6], genetic algorithms (GA) [15], unscented Kalman filters [16], the particle swarm optimization method [10] as well as hybrid methods combining GA and NLS algorithms, such as the Levenberg-Marquardt [4], are widely used for dynamic load modeling.

However, since standard load models cannot capture accurately the underlying dynamic phenomena of power system loads [17], researchers have demonstrated a strong interest in artificial-intelligence modeling techniques, such as neural networks [18], population diversity GAs [19], and fuzzy systems [20]. These techniques are able to identify suitable mathematical representations, which relate efficiently the inputs and outputs of the developed model without assuming any predefined standard load model structure. However, such approaches present certain shortcomings and limitations, mainly related to the slow convergence rate, the inaccurate determination of the initial conditions, and the training failures caused by the emergence of local minima [4], [17]. Furthermore, the associated model parameters vary significantly during different loading conditions and voltage disturbances. As a result, the parameter updating procedure may become extremely time-

consuming, prohibiting the use of such models in real time applications.

In this paper, a new variable-order aggregate load model is proposed to overcome the above issues. The proposed model is formulated with an input/output [9], [21] structure, based on the well-established exponential recovery load model (ERLM) formulation [11], [22]. Contrary to the standard, first-order form of the ERLM, the proposed model employs variable-order transfer functions. As a result, it can capture accurately the oscillatory behavior of complex power system loads. Additionally, a complete and compact methodology for the automatic derivation of the minimum-required model order is proposed, enhancing this way the applicability of the developed model to real applications, while also facilitating the development of low-order dynamic load models. Moreover, to derive robust model parameters, a transparent multi-signal identification procedure is developed, which exploits the vast amount of data captured from PMUs. For this purpose, the Vector Fitting (VF) method is introduced, for the first time, as a technique for measurement-based load modeling. Initially, the accuracy of the proposed model is investigated using simulated responses, obtained from two large-scale power systems by applying the Monte Carlo (MC) method. Detailed time-domain (TD) simulations using the complete network models of the IEEE 39-Bus and the IEEE 68-Bus test systems are performed through the NEPLAN software [23]. Simulated responses are used, instead of measurements, for the development of the proposed aggregate load model. The applicability of the proposed model is also demonstrated using measurements recorded on a laboratory-scale microgrid. Finally, the generalization capability of the proposed model is evaluated using the cross-validation technique [7], [14], while its performance is thoroughly compared with other conventional load models, revealing its superiority in the dynamic simulation of complex power system loads.

II. Theoretical Background

The mathematical formulation of the ERLM and VF algorithm are briefly reviewed in this section to provide the appropriate background for the proposed model.

A. The Exponential Recovery Load Model

The mathematical expression of the ERLM is defined as [11], [22]:

$$y_d(t) = y_r(t) + f_1(V_L(t)) \tag{1}$$

$$T_y \dot{y}_r(t) + y_r(t) = f_2(V_L(t)) \tag{2}$$

$$f_1(V_L(t)) \equiv y_t(t) \qquad f_2(V_L(t)) \equiv y_s(t) - y_t(t) \tag{3}$$

$$y_s(t) = y_0 \left[\frac{V_L(t)}{V_0}\right]^{N_s} \qquad y_t(t) = y_0 \left[\frac{V_L(t)}{V_0}\right]^{N_t} \tag{4}$$

where y_d is the total load demand of real or reactive power at time t, y_r is the state variable which describes the procedure of the load recovery, and T_y is the time constant of y_r. Furthermore, V_L is the load voltage, while y_s and y_t are two auxiliary functions, associated with the steady-state and the transient nonlinear characteristics of the load, respectively.

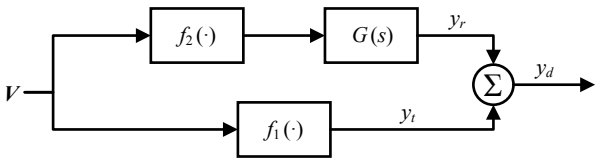

Fig. 1. General block structure representation of the dynamic load model.

Parameters N_s and N_t stand for the steady-state and the transient voltage exponents, respectively, while V_0 and y_0 are the voltage magnitude and the total power consumption prior to the disturbance.

The ERLM can be represented as a block diagram interconnection of two nonlinear functions and a first-order linear transfer function [11], as shown in Fig. 1. Specifically, the lower branch of the block diagram representation is a nonlinearity, expressed with function f_1, describing the transient part of the real or/and reactive power response in watts (W) and vars (VAr), respectively [6], [9], [11], [22]. This nonlinearity has as input the time-varying voltage $V_L(t)$ as shown in (3) and (4). On the other hand, the upper branch consists of two distinct components: The first part, described by function f_2, is another nonlinearity applied to the time-varying input voltage and is also measured in W or VAr. The second component, described by $G(s)$, is a first-order linear transfer function with gain and pole equal to $1/T_y$ and $-1/T_y$, respectively [9]. The $G(s)$ function is used to approximate the recovery response of the real or/and reactive power [11], [22].

B. General Dynamic Load Model Structure

The block diagram representation of the ERLM can be extended to describe higher order load dynamics [11], [22]. In this case, the load nonlinearities are modeled using the nonlinear functions f_1 and f_2 of (3), while the load recovery is approximated using a linear transfer function with the general high-order form:

$$G(s) = \frac{\beta_\nu s^\nu + \beta_{\nu-1} s^{\nu-1} + ... + \beta_0}{s^\mu + \alpha_{\mu-1} s^{\mu-1} + ... + \alpha_0} \tag{5}$$

The only restriction applied to this case is that $G(s)$ should be strictly proper, i.e., $\nu < \mu$, to ensure that the load recovery is continuous. To adequately simulate the dynamic behavior of the aggregate load, the optimal order μ of $G(s)$ and the required set of parameters $\boldsymbol{\theta} = [N_s, N_t, \beta_\nu, \beta_{\nu-1}, ..., \beta_0, \alpha_{\mu-1}, ..., \alpha_0]$ must be specified using measurements.

The order of $G(s)$ has a significant impact on the performance and accuracy of the developed load model [11], [24]. However, in the literature there are no specific guidelines to determine the ideal model order in order to simulate complex load dynamics. In fact, the structure of all conventional load models, in real applications [1], [11], [24] is assumed *a priori* known. Therefore, in many cases these models fail to capture accurately the dynamics of power system loads. Furthermore, the required parameters of conventional load models are generally estimated using nonlinear optimization techniques [9], [25]. However, these methods may lead to local minimum

solutions and are very sensitive to noise [25], resulting also in complicated and time-consuming identification procedures.

This paper tackles these issues by developing an iterative procedure for the automatic determination of the optimal model order and by introducing the VF method as a measurement-based load modeling technique. The VF algorithm is employed for the accurate identification of $G(s)$ parameters, avoiding the use of complex nonlinear optimization techniques.

C. The Vector Fitting Technique

The objective of the VF algorithm [26] is to approximate a frequency-domain (FD) response, such as the considered $G(s)$ transfer function of (5), in a pole-residue form:

$$G(s) \simeq \sum_{m=1}^{\mu} \frac{c_m}{s - p_m} \tag{6}$$

where the poles $\{p_m\}$ and residues $\{c_m\}$ are either real quantities or complex conjugate pairs [26].

Given a fixed number of frequency data samples $\{s_k, G(s_k)\}_{k=1}^{K}$, the VF identifies the parameters of (6) by specifying a set of initial poles $\{q_m^{(0)}\}$ for the weighting function of (7). Generally, these initial poles should be chosen to span uniformly in the frequency bandwidth over which the approximation is to be calculated [26].

$$\sigma^{(i)}(s) = 1 + \sum_{m=1}^{\mu} \frac{\tilde{c}_m^{(i)}}{s - q_m^{(i)}} \tag{7}$$

Moreover, the rational approximation of $\sigma^{(i)}(s)G(s)$ is described as:

$$\sigma^{(i)}(s)G(s) \simeq \sum_{m=1}^{\mu} \frac{c_m^{(i)}}{s - q_m^{(i)}} \tag{8}$$

By multiplying (7) with the data values of $G(s)$ and equating with (8) the following system of equations is formulated:

$$\sum_{m=1}^{\mu} \frac{c_m^{(i)}}{s - q_m^{(i)}} = \left(1 + \sum_{m=1}^{\mu} \frac{\tilde{c}_m^{(i)}}{s - q_m^{(i)}}\right) G(s) \tag{9}$$

In the above formulation, $\{q_m^{(i)}\}$ denotes the set of poles at the i-th algorithm iteration, $\{c_m^{(i)}\}$ stands for the corresponding unknown residues, while $\{\tilde{c}_m^{(i)}\}$ are the residues of $\sigma^i(s)$.

For a given frequency data point s_k, the system of (9) is expressed as [26]:

$$\mathbf{A}_k \mathbf{x} = \mathbf{B}_k \tag{10}$$

where $\mathbf{x} = [c_1^{(i)} \ ... \ c_\mu^{(i)} \quad \tilde{c}_1^{(i)} \ ... \ \tilde{c}_\mu^{(i)}]$, while $\mathbf{A}_k$ and $\mathbf{B}_k$ are appropriate matrices, assembled as shown in [27, eq. 6] [27]. Formulating (10) for all the available frequency points leads to the overdetermined linear problem of (11) [26].

$$\mathbf{A}\mathbf{x} = \mathbf{B} \tag{11}$$

$\mathbf{x}$ can be obtained through (11) via a least square solution. Afterward, the zeros $\{\tilde{z}_m^i\}$ of $\sigma^{(i)}(s)$ are computed by solving the eigenvalue problem of (12).

$$\tilde{z}_m^{(i)} = q_m^{(i+1)} = eig\big(\mathbf{P}^{(i)} - \mathbf{b}^{(i)}(\mathbf{c}^{(i)})^T\big) \tag{12}$$

where, $\mathbf{P}^{(i)}$ is a diagonal matrix containing the initial poles, $\mathbf{c}^{(i)}$ is a row vector holding the residues of $\sigma^{(i)}(s)$ and $\mathbf{b}^{(i)}$ is a column vector of ones [26].

It can be shown that the zeros $\{\tilde{z}_m^i\}$ of $\sigma^i(s)$ are equal to the poles of the rational approximation of $G(s)$ [26]. Thus, in each iteration, the zeros calculated via (12), become the new poles $\{q_m^{(i+1)}\}$ which replace the old ones $\{q_m^{(i)}\}$. This procedure is applied iteratively until convergence is achieved at the I_Tth iteration of the algorithm. Once the poles $\{p_m\}$ have been identified, a second least-squares solution of (8) provides the corresponding residues $\{c_m\}$ by setting $\sigma^i(s)$ equal to unity [26], [28]. The iterative procedure of the VF algorithm is further explained in the following pseudocode:

Algorithm 1 Pseudocode for the Vector Fitting (VF) algorithm

1: Extract $G(s)$
2: Set $i = 0$ and assign $q_m^{(0)}$
3: **repeat**
4: Calculate $\{\tilde{c}_m^{(i)}\}$ by solving (11)
5: Calculate $\{q_m^{(i+1)}\}$ by solving (12)
6: $i = i + 1$
7: **until** $\{q_m^{(i)}\}$ converges after I_T iterations
8: Calculate $\{c_m^{(I_T)}\}$ via (8) by setting $\sigma^i(s)$ equal to unity

In [28], a modification of the VF algorithm is introduced by changing the weighting function of (7) to the following one:

$$\sigma^i(s) = \tilde{d}^i + \sum_{m=1}^{\mu} \frac{\tilde{c}_m^i}{s - q_m^i} \tag{13}$$

and by adding (14) as an additional equation to the resulting least-square problem of (11).

$$Re\left\{\sum_{k=1}^{K}\left(\tilde{d}^i + \sum_{m=1}^{\mu}\frac{\tilde{c}_m^i}{s_k - q_m^i}\right)\right\} = K \tag{14}$$

In this case, (9) is transformed to (15), while matrices $\mathbf{x}$, $\mathbf{A}_k$ and $\mathbf{B}_k$ are assembled as shown in [27, eq. 14] [27]. Finally, the required zeros $\tilde{z}_m^{(i)}$ are computed using (16). This modification is generally used to enhance the convergence of the VF algorithm [27]–[29].

$$\sum_{m=1}^{\mu} \frac{c_m^{(i)}}{s - q_m^{(i)}} = \left(\tilde{d}^{(i)} + \sum_{m=1}^{\mu} \frac{\tilde{c}_m^{(i)}}{s - q_m^{(i)}}\right) G(s) \tag{15}$$

$$\tilde{z}_m^{(i)} = q_m^{(i+1)} = eig\big(\mathbf{P}^{(i)} - \mathbf{b}^{(i)}(\tilde{d}^{(i)})^{-1}(\mathbf{c}^{(i)})^T\big) \tag{16}$$

In this paper, using the VF algorithm, the rational approximation of the $G(s)$ transfer function is computed by means of a two-stage linear least squares solution, avoiding this way the use of time-consuming, nonlinear optimization techniques.

III. Proposed Load Modeling Procedure

The proposed load model adopts the general block structure of Fig. 1, treating real and reactive power as independent quantities. Voltage disturbances are considered as inputs of the model, while the output includes the real and the reactive power response. Load nonlinearities are simulated using the exponential functions f_1 and f_2, while the load recovery

response is approximated using a variable-order linear transfer function. The optimal order of the required transfer function is automatically determined using the iterative procedure of Fig. 2, while the corresponding parameters are estimated using the VF technique.

More specifically, the algorithm of the proposed model consists of two main stages: At the first stage, data preprocessing is applied to all measured signals, while at the second stage, the load model parameters are calculated achieving a minimum required model order. The rest of this section describes in detail the proposed procedure.

A. Signal Recording and Data Preprocessing

The proposed method is designed for the development of load models using the measurement-based approach. For this purpose, when a voltage disturbance occurs, the resulting voltage and current responses can be recorded using PMUs or power analyzers and the corresponding real and reactive power responses are computed. In real field conditions, the signals of real and reactive power $y_{m,d}[n]$ contain, apart from the pure signal $y_d[n]$, the additive noise $\epsilon[n]$ [7], [30] as described by:

$$y_{m,d}[n] = y_d[n] + \epsilon[n] \tag{17}$$

Preprocessing is performed prior to the parameter estimation, to filter out high-frequency components, caused by harmonics and noise [31]. The recorded responses are first up-sampled by means of the shape-preserving piecewise interpolation technique [32] to enhance the quality of the measured data. Afterward, signals are processed through finite impulse response (FIR), zero-phase, low-pass filters (LPF) with adjustable cut-off frequencies, to increase the signal-to-noise (SNR) ratio. For real field applications, cut-off frequencies can be determined from historical network data.

B. Parameter Estimation

At this stage, the processed signals of voltage, real and reactive power are used to estimate the required model parameters. To find the minimum required model order, the following iterative procedure is adopted:

Step-1: Initially, the values of voltage exponents N_s and N_t, shown in (4), are determined using the following equations [11]:

$$N_s = \frac{log\left(\frac{y_{ss}}{y_0}\right)}{log\left(\frac{V_{ss}}{V_0}\right)} \qquad N_t = \frac{log\left(\frac{y_+}{y_0}\right)}{log\left(\frac{V_+}{V_0}\right)} \tag{18}$$

where V_{ss} and y_{ss} denote the voltage magnitude and load consumption at the new steady-state, respectively. On the other hand, V_+ and y_+ express the voltage and power immediately after the disturbance.

Step-2: Functions f_1 and f_2 are calculated using (3).

Step-3: The recovery response of the load, i.e. y_r, is extracted from the overall load response using (1).

Step-4: The fast Fourier transform $\mathcal{F}$ of signals y_r and f_2 is computed, using the regular sampling scheme [33].

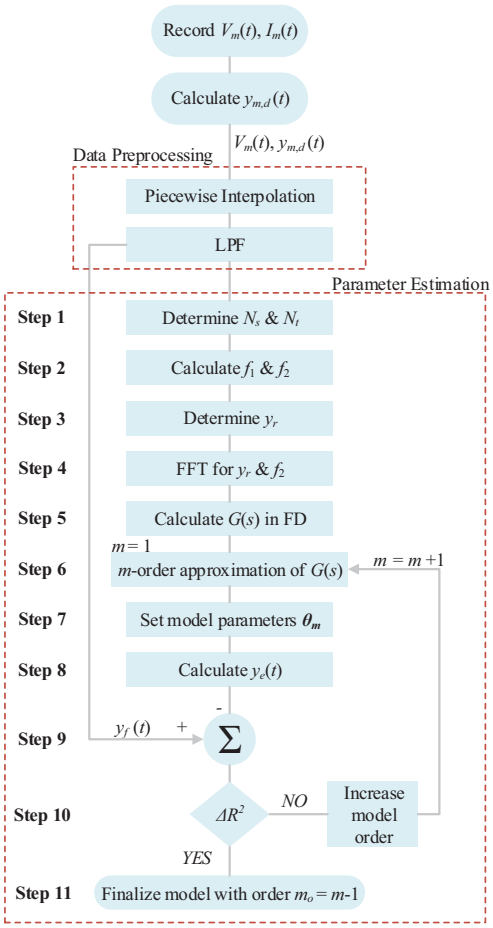

Fig. 2. Flowchart of the proposed load model.

Step-5: The transfer function $G(s)$ is calculated in FD by:

$$G(s) = \frac{\mathcal{F}(y_r)}{\mathcal{F}(f_2)} \tag{19}$$

Step-6: An m-order approximation of $G(s)$, denoted as $\hat{G}(s)$, is calculated using the VF technique.

Step-7: The set of parameters $\boldsymbol{\theta}_m = [N_s, N_t, \boldsymbol{p}_m, \boldsymbol{c}_m]$ is defined, containing the steady-state and transient voltage exponents, as well as the m identified poles and corresponding residues of $\hat{G}(s)$. Here, m stands for the m-th iteration of the proposed algorithm, while initially it is set equal to one.

Step-8: Using the above coefficients, the estimated response $y_e[n]$ is calculated in the TD.

Step-9: The estimated load response is compared to the filtered signal $y_f[n]$ with mean value $\bar{y}_f$, and the coefficient of determination R^2_m is calculated by:

$$R^2_m = \left(1 - \frac{\sum_{n=1}^{N}(y_f[n] - y_e[n|\boldsymbol{\theta}_m])^2}{\sum_{n=1}^{N}(y_f[n] - \bar{y}_f)^2}\right) \cdot 100\% \tag{20}$$

Step-10: The coefficient $\Delta R^2 = R^2_m - R^2_{m-1}$ between the last two iterations of the algorithm is computed and used to check the convergence of the proposed load modeling procedure, since it has been proven an efficient convergence criterion [34]. For the first iteration of the algorithm it is assumed

that the coefficient R_0^2 is equal to zero. If the ΔR^2 criterion is less than a user-defined value, the algorithm proceeds to Step 11. Otherwise, the procedure moves to Step 6 and a new approximation of the $G(s)$ is computed, by setting $m = m+1$.
Step-11: The attainment of ΔR^2 criterion implies that the last iteration of the algorithm is not needed, since the coefficient of determination does not change notably. Thus, the algorithm terminates and the resulting final model order is equal to $m_o = m - 1$.

Based on the previous analysis, it is now clear that the general mathematical expression, used by the proposed model to estimate the real and reactive power, has the following form:

$$y_e(t) = f_1(V_L(t)) + \mathcal{F}^{-1}[\mathcal{F}(f_2)\hat{G}] \tag{21}$$

where:

$$\hat{G}(s) = \sum_{m=1}^{m_o} \frac{c_m}{s - p_m} = \frac{\delta_\xi s^\xi + \delta_{\xi-1} s^{\xi-1} + ... + \delta_0}{s^{m_o} + \gamma_{m_o-1} s^{m_o-1} + ... + \gamma_0} \tag{22}$$

C. Multi-Signal Analysis

Load model parameters vary notably due to distinct loading conditions and change significantly during seasons, weeks and hours of the day [**?**], [14], [35], [36]. Moreover, it is widely accepted that load models derived from a limited number of measurements may be unreliable, since they present low generalization capabilities [7]. Thus, the common practice to enhance the robustness of load models is to calculate, for a close range of loading conditions, representative sets of parameters using multi-signal analysis [7], [14], [35]. For this purpose, in this subsection, the identification procedure of Fig. 2 is extended to develop a complete methodology for the estimation of the required model parameters using multiple data sets.

Given a set of L measurements, a generic set of parameters $\bar{\boldsymbol{\theta}}_m = [\bar{N}_s, \bar{N}_t, \bar{\boldsymbol{p}}_m, \bar{\boldsymbol{c}}_m]$ is estimated, representing a general relation between the model inputs and outputs. Note that $\bar{\boldsymbol{p}}_m$ and $\bar{\boldsymbol{c}}_m$ correspond to the poles and residues of the generic transfer function $\bar{G}(s)$. To calculate the generic set of parameters the following procedure is proposed: First, the data preprocessing of Fig. 2 is performed for all measured signals. Then, Step 1 of the proposed algorithm is applied individually to each data set and L distinct sets of N_s and N_t parameters are determined.

The representative values for the steady-state and transient voltage exponents, denoted as $\bar{N}_s$ and $\bar{N}_t$, are identified from the available measured signals by means of NLS optimization using (4) as the objective function. Specifically, $\bar{N}_s$ and $\bar{N}_t$ are estimated by:

$$min\left\{ \frac{\sum_{l=1}^{L} \left[y_{l,ss} - y_{l,0} \left(\frac{V_{l,ss}}{V_{l,0}} \right)^{\bar{N}_s} \right] W_l}{\sum_{l=1}^{L} W_l} \right\} \tag{23}$$

$$min\left\{ \frac{\sum_{l=1}^{L} \left[y_{l,+} - y_{l,0} \left(\frac{V_{l,+}}{V_{l,0}} \right)^{\bar{N}_t} \right] W_l}{\sum_{l=1}^{L} W_l} \right\} \tag{24}$$

where $V_{l,ss}$ and $y_{l,ss}$ denote the voltage magnitude and load consumption at the new steady-state for each of the L responses. $V_{l,+}$ and $y_{l,+}$ stand for the corresponding voltage and power consumption immediately after each disturbance, while $V_{l,0}$ and $y_{l,0}$ are the voltage magnitude and the load consumption prior to each disturbance, respectively. Moreover, W_l is a weighting factor related with the l-th measurement data set. Since the effect of this weighting factor is practically small, for simplicity in this paper, W_l is set equal to one [14]. However, it is noted that using the proposed formulation different weighting factor assumptions can be readily supported [37].

Generally, the NLS procedure has a fast convergence, but it relies on the initial estimation of the unknown parameters. Depending on this starting guess, local optimum solutions may occur during the optimization process in (23) and (24). To overcome this issue, a scatter-search mechanism for generating starting points is adopted, as proposed in [38] and [39]. In this paper, the initial points are created within a finite range, varying between the minimum and maximum values of N_s and N_t parameters, as acquired from the L distinct data sets.

Subsequently, Steps 2-5 of the proposed algorithm are separately applied to each data set and L individual responses of $G(s)$ are calculated. A generalized linear transfer function $\bar{G}(s)$ is computed, approximating the load characteristics of the L individual $G(s)$. To estimate the coefficients of $\bar{G}(s)$, the L distinct $G(s)$ functions are grouped together and inserted as inputs to the VF algorithm. The original VF method results in a common set of poles $\bar{\boldsymbol{p}}_m$ and L distinct sets of residues [40]. In this work, to calculate a common set of residues $\bar{\boldsymbol{c}}_m$ the following procedure is proposed: The L set of residues, calculated at each algorithm iteration, are grouped according to the related pole. Then, for each group j of residues, a representative value is calculated by means of the following average function [41], [42]:

$$\bar{c}_m^j = \frac{\sum_{l=1}^{L} c_{m,l}^j E_l}{\sum_{l=1}^{L} E_l} \tag{25}$$

where E_l is the energy of the l-th $G(s)$ function [43], calculated by (26), while $c_{m,l}^j$ denotes the j-th residue for the l-th signal at the m-th algorithm iteration.

$$E_l = \sum_{n=1}^{N} |\mathcal{F}^{-1} G_l[n]|^2 \tag{26}$$

where N denotes the total number of TD samples. Instead of E_l, the proposed formulation allows also the use of any other user-defined weighting factor [37].

To determine the minimum-required model order, Steps 6-11 of Fig. 2 are applied. However, in this case, the ΔR^2 criterion is defined as $\Delta R^2 = R_{m,L}^2 - R_{m-1,L}^2$, where $R_{m,L}^2$ is calculated by:

$$R_{m,L}^2 = \frac{1}{L} \sum_{l=1}^{L} R_{m,l}^2 \tag{27}$$

IV. Simulation Study on the IEEE 39-Bus Test System

In this section the accuracy of the proposed load model is evaluated on the IEEE 39-bus test system, using simulations results in the NEPLAN software [23]. More specifically, the robustness of the proposed model is assessed under highly noisy conditions by employing the Monte Carlo (MC) analysis, while its performance is compared with other conventional load models. Finally, the generalization capability of the proposed model is thoroughly evaluated using the cross-validation technique.

A. Determination of the Optimal Model Order

First, the performance of the proposed model and the iterative procedure for the automatic determination of the optimal model order are thoroughly evaluated. More specifically, simulation responses at Bus-12 are used, where an additional load to the original, consisting of induction motors (IMs) and static loads, is connected. The total capacity of the installed IMs is equal to 8.9 MVA, while the rated power of the static loads is considered equal to 2.2 MVA. The third-order induction machine model is employed for the modeling of the installed IMs, while the static load is modeled as a constant impedance load. To investigate load dynamics, a -3% voltage step disturbance is caused, using an ideal on-load-tap-changer (OLTC) transformer [10]. This procedure is widely used for the development of dynamic load models [11], [35], [44], [45] and is also adopted in this paper, since disturbances caused by transformer tap changing can capture the load characteristics that are critical for power system stability studies [45].

The real and reactive power responses as well as the voltage magnitude of the corresponding load bus are acquired at a data rate of 100 samples per second (sps) to replicate a realistic PMU data stream. Afterwards, in order to simulate real field conditions, the original signals, obtained by detailed simulations using the NEPLAN software, are intentionally distorted by additive white Gaussian noise (AWGN) [6], assuming a SNR equal to 30 dB. Finally, the noisy signals are up-sampled to 1000 sps, filtered using LPFs and used as inputs for the development of the proposed load model.

The convergence rate of the proposed iterative procedure is analyzed in Table I. Considering the modeling of the real power, at the third iteration of the algorithm the coefficient of determination R_3^2 is equal to 99.73% and the corresponding ΔR^2 criterion is 2.04%. Assuming a ΔR^2 criterion equal to 5%, the algorithm completes at this stage and the resulting model order is equal to two, i.e., $m_{o,p} = 2$. Thus, a second-order linear transfer function is employed for the representation of the recovery response of the real power. Considering a stricter ΔR^2 criterion, e.g. 1%, an additional fourth iteration is required, resulting in a third-order model, i.e., $m_{o,p} = 3$. On the other hand, concerning the modeling of the reactive power, the corresponding ΔR^2 criterion for the second iteration of the algorithm is merely 0.71%. Thus, the reactive power can be efficiently modeled using a first-order transfer function, i.e., $m_{o,q} = 1$.

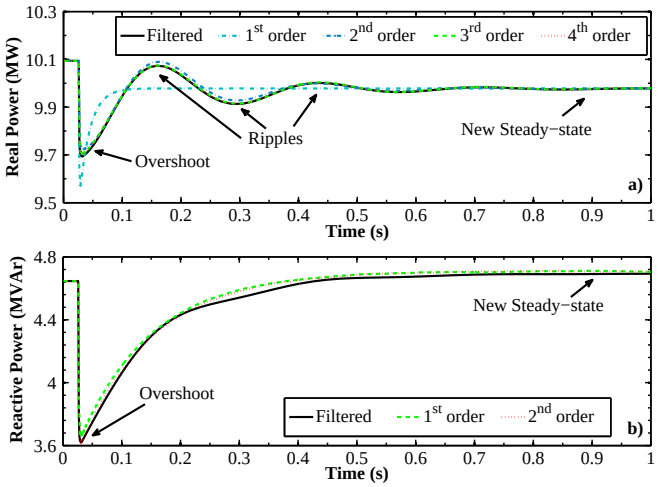

Fig. 3. Simulation of the a) real and b) reactive power response, assuming different model orders.

The modeling of real and reactive power are further analyzed in Figs. 3a and 3b, respectively. The estimated responses calculated by the proposed model are compared with the corresponding filtered signals, obtained using detailed TD simulations. In each case, distinct number of iterations for the proposed algorithm are considered, resulting in different model orders. The obtained voltage exponents for each case, as well as the corresponding poles and residues for each algorithm iteration, are presented in Tables II and III.

The reactive power response, presented in Fig. 3b, can be analyzed into two distinct parts. In the first part an instantaneous power overshoot, related with the abrupt voltage change, is observed, while during the second phase the new steady-state is gradually established. This behavior can be easily modeled using a first-order model.

TABLE I
Convergence Rate of the Proposed Iterative Procedure

	Modeling of real power	
Iteration	$\boldsymbol{R^2}$ **(%)**	$\boldsymbol{\Delta R^2}$ **(%)**
m = 1	56.45	56.45
m = 2	97.69	41.24
m = 3	99.73	2.04
m = 4	99.78	0.05
	Modeling of reactive power	
Iteration	$\boldsymbol{R^2}$ **(%)**	$\boldsymbol{\Delta R^2}$ **(%)**
m = 1	98.55	98.55
m = 2	99.25	0.71

TABLE II
Parameters for Real Power Modeling

Exponents	$\boldsymbol{N_s}$	$\boldsymbol{N_t}$
Value	0.38	1.35
Iteration	$\boldsymbol{p_m}$	$\boldsymbol{c_m}$
m = 1	-5.60	1300.6
m = 2	-6.22 $\pm$ $j2\pi$3.73	346.49 $\pm$ j114.11
m = 3	-7.1, -5.17 $\pm$ $j2\pi$3.62	145.38, 307.95 $\pm$ j31.29
m = 4	-0.006, -6.81, -5.2 $\pm$ $j2\pi$3.63	-0.17, 136.63, 314.35 $\pm$ j38.91

TABLE III
PARAMETERS FOR REACTIVE POWER MODELING

Exponents	N_s	N_t
Value	-0.33	8.28
Iteration	p_m	c_m
m = 1	-8.08	792.4
m = 2	-0.02, -8.11	-1.86, 830.81

The real power response can be also analyzed in two distinct phases. Similar to the reactive power, in the first part an instantaneous power overshoot is observed, while in the second phase the new steady-state is gradually established. However, during the second part of the real power response, several ripples are also observed. As shown, a first-order model, corresponding to the conventional ERLM, cannot represent adequately this dynamic behavior. To capture this oscillatory response of the load, second-, third-, and/or fourth-order models can be used. The optimal model order dependents on the desired accuracy and can be easily determined by the proposed load modeling procedure. As shown in Table I, the accuracy of the developed model can be enhanced by reducing the value of the ΔR^2 criterion.

To further demonstrate the proposed procedure, the modeling of the real power response is analyzed step-by-step. More specifically, in Step 1 of the algorithm, the required voltage exponents N_s and N_t are determined from the filtered signals. In Step 2, the responses of the nonlinear functions f_1 and f_2 are calculated in the TD. The corresponding results are illustrated in Figs. 4a and 4b, respectively. Subsequently, Steps 3-5 are employed and the $G(s)$ function is extracted in the FD. The magnitude and angle of the corresponding $G(s)$ are presented in Figs. 5a and 5b, respectively. Afterward, in Step 6, an m-order approximation of the $G(s)$ is calculated using the VF method. As shown, the $G(s)$ cannot be sufficiently estimated by a first-order approximation. Thus, in each iteration of the proposed algorithm, new poles and residues are added, resulting into higher accuracy in the approximation of $G(s)$. In the remaining Steps of the algorithm, the estimated real power responses are calculated in the TD and compared with the corresponding filtered signal, as shown in Fig. 3a.

The poles of the linear transfer functions, used to approximate the $G(s)$, characterize the modes and thus the dynamic behavior of the examined network. Therefore, to further evaluate the accuracy of the proposed method, the poles of the employed linear transfer functions are compared with the critical eigenvalues of the system. To compute the true system modes, the detailed network model is linearized, using the eigenvalue analysis module of the NEPLAN software [23]. The system under consideration has an oscillatory mode at 3.615 Hz with a damping factor equal -5.237 s^{-1} as well as a DC mode with damping factor -7.396 s^{-1}. As shown in Tables II and III, the pole estimates provided by the proposed method, are very close to the true system eigenvalues, acquired using the detailed linearized network model, validating this way the accuracy of the proposed modeling procedure.

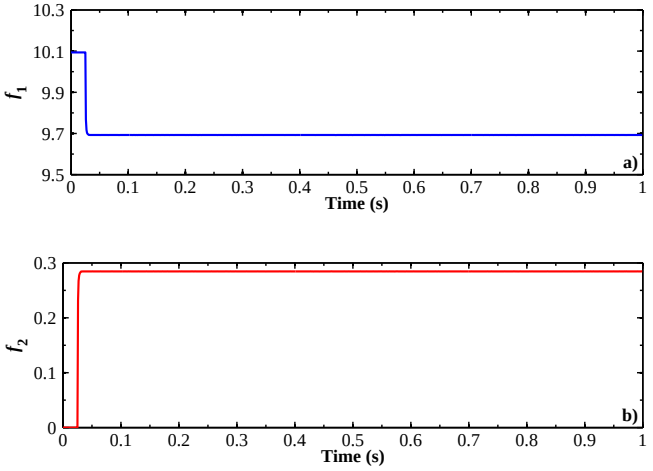

Fig. 4. Modeling of the real power. TD responses of the required voltage-dependent nonlinear functions a) f_1 and b) f_2.

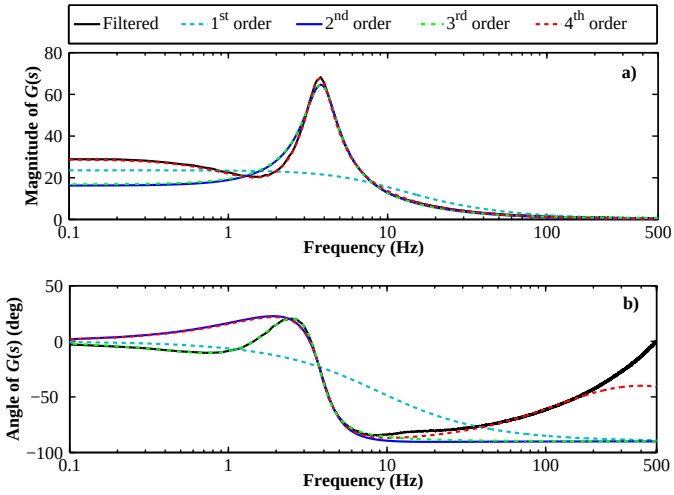

Fig. 5. Modeling of real power. Approximation of the $G(s)$. a) Magnitude and b) angle.

B. Parameter Estimation under Noisy Conditions

In this subsection, MC simulations are employed to evaluate the effectiveness of the proposed method under highly noisy environments. For this purpose, the original signals of real and reactive power, acquired from the NEPLAN software, are distorted with AWGN, the variance of which is adjusted to represent discrete SNR levels varying from 10 to 30 dB. For each noise level, 100 MC simulations are performed, using an Intel Core i7-4770, 3.4 GHz, RAM 8 GB personal computer, to statistically evaluate the performance of the proposed method. Representative results for the three distinct SNR levels are illustrated in Tables II and III, where the mean (μ) and standard deviation (std) of the corresponding R^2, the resulting model order as well as the required execution time for the modeling of the real and reactive power are presented. Note that in all cases a ΔR^2 criterion equal to 5% is considered for the estimation of the model parameters.

As shown in Tables IV and V, the proposed method ensures the accurate representation of both real and reactive power, even in highly noisy environments. This is verified by the mean

TABLE IV
MODELING OF REAL POWER

	R_p^2 (%)		$m_{o,p}$		Time (s)	
SNR	μ	std	μ	std	μ	std
30 dB	97.58	0.09	2	0	0.87	0.18
15 dB	97.11	0.48	2	0	0.93	0.17
10 dB	94.84	0.85	2	0	1.08	0.19

TABLE V
MODELING OF REACTIVE POWER

	R_q^2 (%)		$m_{o,q}$		Time (s)	
SNR	μ	std	μ	std	μ	std
30 dB	98.45	0.06	1	0	0.60	0.13
15 dB	98.22	0.33	1	0	0.61	0.14
10 dB	97.24	0.72	1	0	0.64	0.13

values of the corresponding coefficients of determination, denoted as R_p^2 and R_q^2, which are considerably high in all examined cases.

In all MC simulations, the real power response is satisfactorily simulated by the proposed method using second-order transfer functions. These transfer functions have an oscillatory set of poles and residues. To provide a thorough insight in the variability of these parameters, the scatter diagrams of Figs. 6a and 6b are employed. On the other hand, in all MC simulations, a first-order transfer function with a real pole and residue is considered adequate for the modeling of the reactive power behavior. The possible values of the corresponding poles and residues are presented in the boxplots of Figs. 6c and 6d, respectively. Finally, the range of the required voltage exponents, used for the modeling of the real and reactive power, is depicted in the scatter diagrams of Figs. 6e and 6f, respectively. From all results it is obvious that as the SNR level increases, the variability of the required model parameters is significantly reduced. Moreover, it is evident that even for considerably low SNR levels, the required parameters range in a narrow interval, highlighting the robustness of the proposed load modeling procedure.

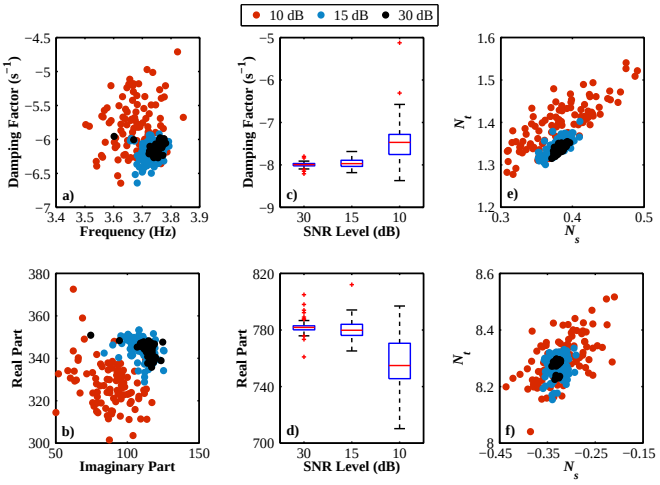

Fig. 6. Variability of model parameters. a) Poles and b) residues required for the modeling of the real power. Only the positive imaginary parts of poles and residues are plotted. c) Poles and d) residues required for the modeling of the reactive power. Voltage exponents of e) real and f) reactive power.

Concerning the computational burden of the proposed method, the mean execution time for the modeling of the reactive power ranges from 0.60 s to 0.64 s, revealing the feasibility of the developed method for close to real-time applications. Similar results are also observed for the real power. However, in this case slightly higher execution times are recorded, since a second-order model is employed, requiring one more iteration compared to the reactive power case.

C. Comparison with Conventional Load Models

The performance and accuracy of the proposed load modeling procedure is compared with the static polynomial (ZIP) [2] and exponential (EXP) [2] models, which are mostly used by system operators and utilities for stability studies [3]. It is also compared with dynamic models, namely the first-order dynamic ERLM as well as with two composite load models. The composite load model structures include the ZIP and EXP load models, augmented with difference equations [46], denoted as DZIP and DEXP, respectively.

The mathematical representation of the conventional ERLM is defined in (1)-(4), while the mathematical formulation of the static load models is presented in (28)-(29).

$$y_{EXP} = y_0 \left(\frac{V}{V_0}\right)^{\chi_0} \tag{28}$$

$$y_{ZIP} = y_0 \left[\chi_1 \left(\frac{V}{V_0}\right)^2 + \chi_2 \left(\frac{V}{V_0}\right) + \chi_3\right], \quad \sum_{i=1}^{3} \chi_i = 1 \tag{29}$$

where y_{ZIP} and y_{EXP} denote the real or reactive power responses estimated by the ZIP and EXP models, respectively. Moreover, V is the load voltage, while y_0 and V_0 are the total power consumption and voltage magnitude prior to the disturbance. Coefficients, χ_0 as well as χ_1, χ_2 and χ_3 are the parameter sets which must be identified for each load model.

The composite load models incorporate both static and dynamic characteristics of the load. The static load characteristics are represented by the conventional ZIP or EXP models, while the dynamic load characteristics are represented by difference equation models, as shown in (30)-(31).

$$y_{DZIP} = \chi_{\kappa_1} y_{ZIP} + \chi_{\kappa_2} \Delta y[n], \quad \sum_{i=1}^{2} \chi_{\kappa_i} = 1 \tag{30}$$

$$y_{DEXP} = \chi_{\lambda_1} y_{EXP} + \chi_{\lambda_2} \Delta y[n], \quad \sum_{i=1}^{2} \chi_{\lambda_i} = 1 \tag{31}$$

where χ_{κ_1} and χ_{κ_2} as well as χ_{λ_1} and χ_{λ_2} are composition percentages of static and dynamic load characteristics, respectively. In the general case, $\Delta y[n]$ can be described by variable order difference equation models. However, in order to provide consistent comparisons with the proposed model, first- and second-order difference equation models are used to model the reactive and real power, respectively. The form of these models is described below:

First-order:

$$\Delta y[n] = \chi_{a1}\Delta y[n-1] + \chi_{c0}\Delta V[n] + \chi_{c1}\Delta V[n-1] \quad (32)$$

Second-order:

$$\begin{aligned}\Delta y[n] = \chi_{a1}\Delta y[n-1] + \chi_{a2}\Delta y[n-2] + \\ \chi_{c0}\Delta V[n] + \chi_{c1}\Delta V[n-1] + \chi_{c2}\Delta V[n-2]\end{aligned} \quad (33)$$

The parameters of the ERLM, ZIP, EXP, DZIP and DEXP, are determined using the NLS optimization, targeting to minimize the following objective function:

$$J(X) = \sum_{n=1}^{N}(y_f[n] - \hat{y}[n])^2 \quad (34)$$

where X stands for the required parameter vector. For ZIP, EXP, DZIP and DEXP the initial values of X are taken from [46], while for the ERLM the initial values of X are determined as in [11]. Moreover, N is the total number of samples in TD, while $y_f[n]$ and $\hat{y}[n]$ denote the filtered and the estimated real or reactive power at the n-th sample, respectively.

To thoroughly evaluate the performance of all examined load models, the MC simulations of Section IV.B are considered. Indicative results for the modeling of the real power are presented in Table VI, assuming a SNR level equal to 30 dB. A representative instance of the MC simulations is illustrated in Fig. 7. Due to the fact that both ZIP and EXP models are static load models, they fail to replicate the dynamic behavior of the load, estimating accurately only the new steady-state. On the contrary, the dynamic ERLM captures adequately the overshoot and the new steady-state of the load. Nevertheless, it is evident that the ERLM cannot represent sufficiently the oscillatory behavior of the load, since it is a first-order model. The proposed model, as well as the second-order DZIP and DEXP models, simulate accurately the real power response, capturing the overshoot, the oscillations and the new steady-state. Similar remarks are also valid for the reactive power. However, in this case, first-order models are used, since the reactive power response has the general form of Fig. 3. The corresponding results are presented in Table VII.

Results from Tables VI and VII reveal that the proposed model offers practically the same accuracy with the conventional DZIP and DEXP models. However, these models present certain shortcomings and limitations [46]. More specifically,

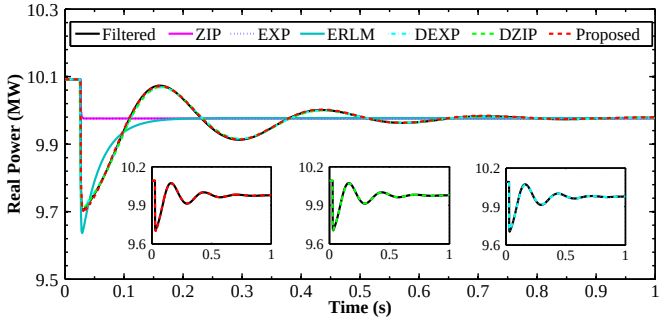

Fig. 7. Filtered and identified real power response.

TABLE VI
MODELING OF REAL POWER. COMPARISONS WITH CONVENTIONAL LOAD MODELS

SNR = 30 dB	R_p^2 **(%)**		**Time (s)**	
Model	μ	std	μ	std
Proposed (2^{nd} order)	97.58	0.09	0.87	0.18
DZIP (2^{nd} order)	98.13	0.91	0.52	0.18
DEXP (2^{nd} order)	97.84	1.01	1.46	1.19
ERLM	67.38	0.15	0.19	0.02
ZIP	1.72	0.02	0.03	0.01
EXP	1.72	0.02	0.02	0.01

TABLE VII
MODELING OF REACTIVE POWER. COMPARISONS WITH CONVENTIONAL LOAD MODELS

SNR = 30 dB	R_p^2 **(%)**		**Time (s)**	
Model	μ	std	μ	std
Proposed (1^{st} order)	98.45	0.06	0.60	0.13
DZIP (1^{st} order)	99.41	0.03	0.30	0.08
DEXP (1^{st} order)	99.92	0.01	1.25	0.12
ERLM	99.79	0.01	0.08	0.03
ZIP	17.03	0.01	0.04	0.03
EXP	17.03	0.01	0.03	0.02

the parameters of these models are generally estimated using NLS optimization techniques. These techniques may lead to local minimum solutions, depending on the initial conditions [4], [9], [25], [46]. Therefore, the performance of these models is strongly related to the optimal selection of the starting points. This issue is further demonstrated in Table VIII, where the resulting R_p^2 for the DZIP model is presented, assuming different initial points for the required set of parameters. In all examined cases, the initial points are generated on a strict interval, ranging from 0 up to 2. However, it is clear that in many cases the optimization procedure is trapped in local minima and the model fails to provide consistent results. A second drawback of these models is the high sensitivity of their parameters to noise, which limits their generalization capabilities. This can be also verified from the results of Table IX, where the parameters of the DEXP model are presented for five random cases of MC simulations. Results reveal that certain parameters are highly affected by noise. Finally, another drawback of these models lies on the fact that their parameters do not have any physical meaning [46].

TABLE VIII
MODELING OF REAL POWER. EFFECT OF INITIAL CONDITIONS ON THE PERFORMANCE OF THE DZIP MODEL

$[\chi_{\kappa 1}, \chi_{\kappa 2}, \chi_1, \chi_2, \chi_3, \chi_{a1}, \chi_{a2}, \chi_{c0}, \chi_{c1}, \chi_{c2}]$	R_p^2 **(%)**
[0.50, 0.50, 0.40, 0.30, 0.30, 1, 2, 1.40, 1.30, 2]	98.27
[0.18, 0.82, 0.42, 0.15, 0.42, 1.83, 1.41, 1.12, 0.63, 0.33]	69.43
[0.76, 0.24, 0.42, 0.48, 0.1 , 1.48, 0.21, 1.36, 0.92, 0.42]	43.77
[0.88, 0.12, 0.13, 0.87, 0, 1.65, 0.79, 1.22, 1.64, 1.77]	29.36
[0.69, 0.31, 0.25, 0.26, 0.48, 0.18, 0.02, 0.85, 1.31, 1.44]	18.69

TABLE IX
MODELING OF REAL POWER. VARIABILITY OF DEXP MODEL PARAMETERS DUE TO THE NOISE

$[\chi_{\lambda 1}, \chi_{\lambda 2}, \chi_0, \chi_{a1}, \chi_{a2}, \chi_{c0}, \chi_{c1}, \chi_{c2}]$	R_p^2 (%)
[0.98, 0.02, 0.23, 3.19E-06, 57.99, 226.31, 23.44, 28.49]	98.99
[0.98, 0.02, 0.48, 1.71E-05, 51.89, 81.13, 1.25, 3.24]	98.81
[0.97, 0.03, 0.51, 3.50E-06, 47.13, 30.61, 1.54, 12.47]	98.61
[0.95, 0.05, 0.51, 8.22E-06, 44.06, 0.32, 0.1E-02, 3.99]	98.41
[0.96, 0.04, 0.49, 5.94E-06, 44.57, 15.56, 2.66, 0.61]	98.44

These limitations are efficiently tackled by the proposed load modeling procedure. First of all, based on the analysis of Section IV.B it is evident that the parameters of the proposed model are not considerably affected by noise. Moreover, the poles of the required transfer functions determine the modes of the examined network, thus offering a significant direct physical interpretation. However, the most important advantage of the proposed method is the independence of the required model parameters from any arbitrary initial guess. The required voltage exponents are determined using simple algebraic equations, while the required poles and residues are estimated using the VF technique, thus avoiding the use of NLS optimization techniques, which may result in sub-optimal solutions.

Finally, results from Tables VI and VII show that the mean execution time for the DEXP model is almost two times greater than the corresponding for the proposed method. On the other hand, the computational burden of the proposed method is slightly higher compared to the DZIP model. This is due to the fact that in all MC simulations the structure of the DZIP and the DEXP models is considered *a priori* known, while in the proposed method the optimal model order is determined automatically for each MC simulation through several iterations. Furthermore, the parameter estimation for the DZIP and the DEXP models is performed using filtered signals as inputs, while, as shown in Fig. 2, the inputs of the proposed method are pure, measured signals. The preprocessing and filtering of these signals, performed by the proposed method prior to the parameter estimation increases the execution time.

D. Generalization Capability

The robustness of the proposed model is thoroughly assessed using the cross-validation technique [7], [14]. Assuming there are available D measurement data sets, the cross-validation method is applied as follows: The given measurement data sets are divided into two separate groups. The first group constitutes the training data set and contains $D-1$ of the acquired measurements. The second group contains the validation data. The required model parameters are estimated based on the training data by employing the proposed multi-signal analysis method. The accuracy of the developed model on the training data is assessed using the coefficient of determination R_{tr}^2, calculated using (27). Afterward, the ability of the developed model to fit new, unseen data is evaluated using the validation data by computing the corresponding coefficient of determination R_v^2. This procedure is repeated D times, until all measured signals are used as validation data. When all D calculations are completed, the average values of the R_{tr}^2 and R_v^2 coefficients are calculated [14].

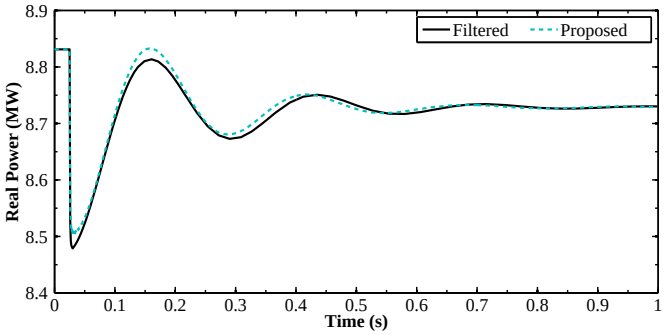

Fig. 8. Instance of the validation procedure.

TABLE X
STATISTICAL EVALUATION FOR THE IEEE 39-BUS SYSTEM

	Real power		Reactive power	
	μ	std	μ	std
R_{tr}^2 (%)	92.05	1.64	91.25	2.58
R_v^2 (%)	91.18	2.05	89.79	3.28

Initially, the robustness of the proposed model is evaluated using simulations results acquired from Bus-12 of the IEEE 39-bus system. The training and the validation data sets are generated by applying distinct voltage disturbances using the OLTC transformer and by altering the rated power of the loads connected to Bus-12. More specifically, the voltage disturbances vary from -0.1 p.u. up to 0.1 p.u., while the total capacity of the installed loads ranges from 8.9 MVA up to 13.3 MVA in order to simulate the time-varying nature of power system loads. Following this approach 36 distinct disturbances are generated. Using a second-order model for the representation of the real power, the average values for the coefficients R_{tr}^2 and R_v^2 are 92.58% and 90.5%, respectively. On the other hand, for the simulation of the reactive power a first-order model is employed and the corresponding coefficients are equal to 92.44% and 91.44%. Therefore, it can be concluded that the proposed model preserves its high accuracy on both training and validation data. In Fig. 8 one instance of the validation procedure is illustrated. As shown, the proposed model simulates very accurately the dynamic behavior of the load, highlighting the robustness and the generalization capability of the developed method.

Similar simulations are conducted for the remaining load buses of the network to statistically evaluate the overall performance of the proposed model. The mean and standard deviation of the acquired R_{tr}^2 and R_v^2 coefficients from the whole training and validation data sets, respectively, are given in Table X. Based on the presented results it is evident that the proposed model preserves its high accuracy in different simulation scenarios, while the high mean value of the R_v^2 coefficient highlights the ability of the developed model to fit adequately new, unseen data.

V. Application on the IEEE 68-Bus Test System

In this Section, the accuracy and effectiveness of the proposed model are further validated by conducting simulations on the IEEE 68-bus system. Also in this case, the detailed network model of the IEEE 68-bus test system is implemented in the NEPLAN software and consists of 68 buses, 16 generators, 19 transformers and 35 loads. The performance of the proposed model is assessed using simulation responses acquired from Bus-39, where the original static load is replaced with 200 induction motors of diverse characteristics. More specifically, six different types of motors are considered: Large (M1) and small (M2) industrial motors, pumps (M3), weighted aggregated models of residential (M4), weighted aggregated models of residential and industrial (M5) motors as well as weighted aggregated motors dominated by air conditioning (M6). The required parameters for the detailed modeling of each motor type are taken from [1].

The effectiveness of the proposed method is thoroughly evaluated using the MC method. For this purpose, an OLTC transformer is used and 100 voltage disturbances, varying from -0.1 p.u. up to 0.1 p.u. are considered. Moreover, in each MC simulation, the composition of the motors is altered and thus a diverse range of distinct network configurations is examined. To accomplish this, the number of induction motors corresponding to a specific motor type, is determined by a weighting factor w_{fi}, ranging from 0% to 100%. For example, a w_{f1} equal to 10% indicates that the total number of large industrial motors (M1) is set to 20. For each motor type, the w_{fi} is generated randomly assuming a uniform distribution. In all cases the following restriction is applied:

$$\sum_{i=1}^{6} w_{fi} = 100\% \tag{35}$$

In each MC simulation, the signals acquired from the NEPLAN software, using the detailed network model, are intentionally distorted by AWGN, assuming SNR equal to 30 dB and are used as inputs to the proposed model. The statistical evaluation of the MC results is given in Table XI, where the mean and standard deviation of the acquired R_p^2 and R_q^2 for the real and reactive power, respectively, are presented. Based on the results, it is clear that the proposed model can simulate very accurately the dynamic behavior of complex power systems, where several types of induction motors are installed. Moreover, four instances of the corresponding MC simulations are illustrated in Fig. 9. The power responses of Bus-39, obtained using detailed TD simulations with the full network model in the NEPLAN software, are compared with the estimates provided by the proposed aggregate load model. Based on these results, it is evident that the proposed model can be used to replace extended parts of complex networks, while it can also be applied to a wide range of distinct configurations, providing very accurate results.

Finally, the performance of the proposed model is investigated for the case of a severe disturbance. A three-phase fault is applied in the middle of line L137, which connects Buses 44 and 45. The fault happens at t = 0.1 s and is cleared after 5 cycles. The voltage at Bus-39, for which the load identification is performed, is presented in Fig. 10a. The calculated real and reactive power responses, using the proposed model, are compared to the corresponding filtered responses, obtained by NEPLAN software in Figs. 10b and 10c, respectively. It is obvious that the proposed model can replicate very accurately the dynamic behavior of the load even under severe disturbances, capturing accurately both the real and reactive power responses.

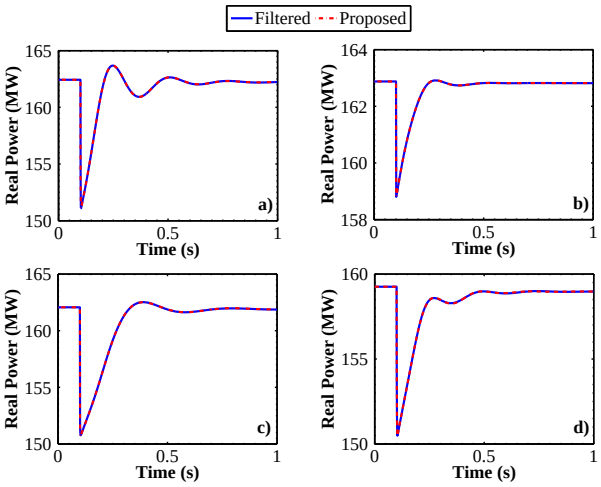

Fig. 9. Four representative instances of the MC simulations conducted on the IEEE 68-Bus test system, assuming distinct motor compositions. a) Pumps are the main type of motors. The dominant type of motors are b) small and c) large industrial. d) Same number of motors is considered for each motor type.

TABLE XI
Statistical Evaluation of MC Simulations On The IEEE 68-Bus System

R_p^2 (%)		R_q^2 (%)	
μ	std	μ	std
98.09	0.87	98.29	1.24

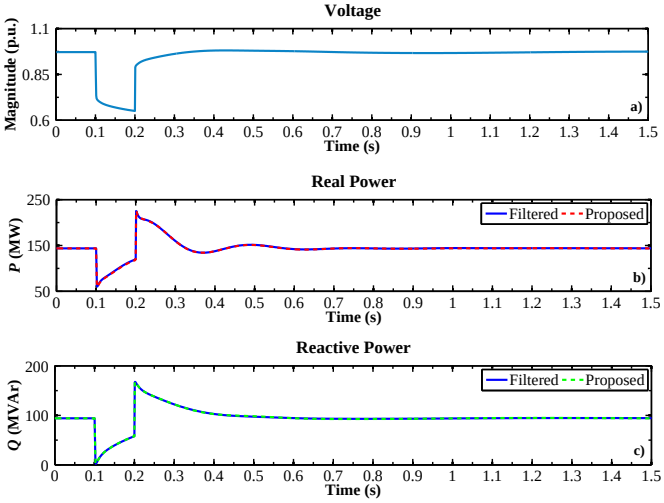

Fig. 10. Modeling of a three-phase fault. a) Voltage magnitude, b) real and c) reactive power response.

VI. Laboratory Measurements

Scope of this section is to evaluate the applicability of the proposed method and to demonstrate its superior performance against the examined composite load models. For this purpose, measurements from a 400 V, 50 Hz, laboratory-scale microgrid (MG) are employed.

The test facility is connected to the utility via a 1.21 p.u. inductance, as illustrated in Fig. 11. The examined MG is modeled as an aggregate load and consists of a three phase 2.2 kW, 0.87 lagging power factor, 400 V asynchronous machine connected in parallel to a three-phase 5 kW, 0.9 lagging power factor, 400 V static load. To investigate load dynamics, four voltage disturbances are caused at the measurement point at Bus-3 by connecting and disconnecting the 256-step, 40 kW/30 kVAr static load bank (LB) at Bus-2. For this purpose, the LB is sequentially connected and disconnected two times with loading conditions equal to 4983 W and 7097 W, respectively, while assuming unity power factor in all disturbances. The signals of voltage magnitude, real and reactive power at Bus-3 are recorded at a data rate of 500 sps and are further processed for the development and validation of the examined load models.

The recorded measurement data sets are divided into two separate groups. The first group constitutes the training data and consists of three of the acquired measurement data sets, while the second group contains the fourth data set, which is used for the cross-validation of the models. The parameters of DZIP and DEXP models are determined for each training data set using the NLS optimization, as discussed in Section IV.C. Afterwards, for each model a generic set of parameters is obtained by computing the corresponding average value of each parameter [30], [31]. On the other hand, the parameters of the proposed method, i.e., the voltage exponents, the required poles and the corresponding residues, are estimated by employing the developed multi-signal approach, assuming a ΔR^2 criterion equal to 5%.

The accuracy of the proposed method on the validation and on the training data sets is verified in Fig. 12, where the percentage relative error of (36) is calculated.

$$Error(\%) = 100\frac{|y_m[n] - y_e[n]|}{y_m[n]} \tag{36}$$

Here, $y_m[n]$ and $y_e[n]$ are the measured and the estimated real or reactive power responses at the n-th sample. Concerning the modeling of the real power, training errors lower than 0.5% are recorded in all cases. Similar results are also observed for the reactive power case, where the corresponding error is lower than 1%. As expected, the validation error for both real and reactive power is slightly higher compared to the corresponding training error. However, the peak values of these errors are merely 0.84% for the real and 1.8% for the reactive power, highlighting the robustness and the generalization capabilities of the proposed method.

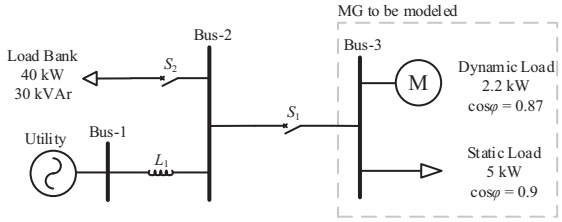

Fig. 11. Laboratory-scale MG experimental setup.

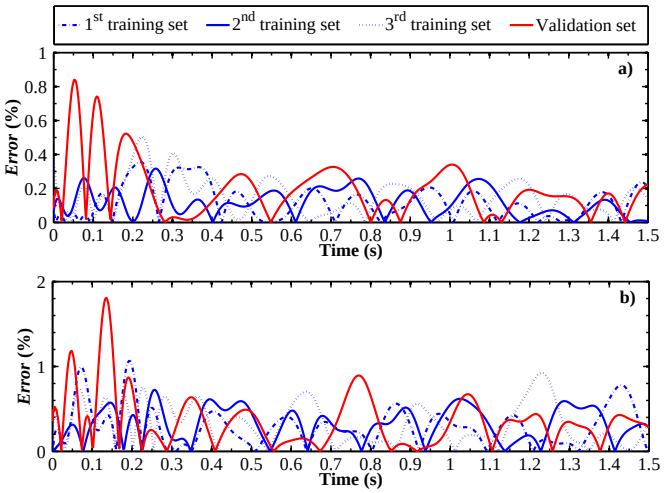

Fig. 12. Relative errors on the training and on the validation set. a) Real and b) reactive power.

The performance of the examined load models on the validation data set is illustrated in Figs. 13 and 14, where the calculated responses are compared to the corresponding measured. As shown, the proposed model presents high accuracy, simulating very adequately the overshoot, the second ripple and the new steady-state of both real and reactive power, by employing two distinct second-order transfer functions. Moreover, based on the presented relative errors as well as the corresponding coefficients of determination, it is clear that the proposed model presents superior performance compared to the DZIP and DEXP models.

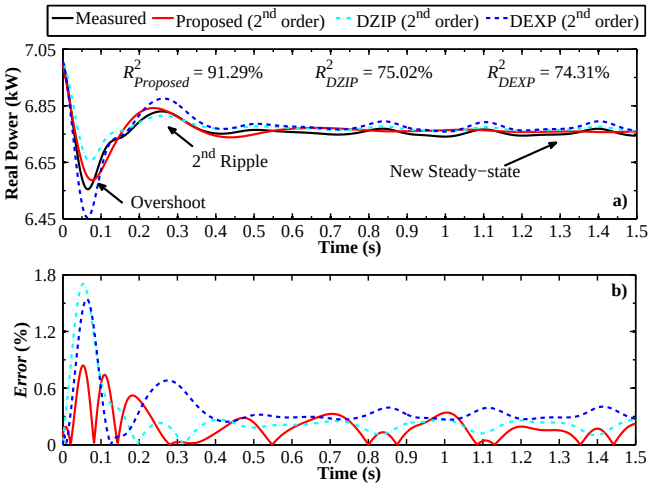

Fig. 13. Measured and identified real power response.

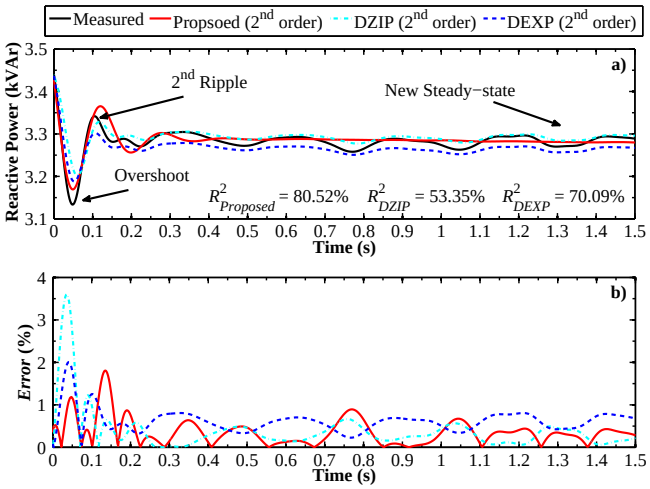

Fig. 14. Measured and identified reactive power response.

VII. Discussion and Conclusions

In this paper, an adjustable input/output load model, suitable for dynamic simulations, is proposed. The new model can capture accurately high-order load dynamics, by employing variable-order linear transfer functions. The VF method is used to accurately identify the coefficients of the required transfer functions. The proposed load modeling procedure is extended to allow multi-signal analysis, exploiting PMU measurements and facilitating the development of robust dynamic load models.

The effectiveness of the proposed model is thoroughly investigated at the the IEEE 39-Bus and the IEEE 69-Bus test systems, using MC simulations. In all examined cases, the proposed model preserves its accuracy, simulating efficiently both the real and reactive power, even in highly noisy environments, combining fast convergence and relatively small execution times. The applicability of the proposed model is tested using measurements from a laboratory-scale MG, while its performance is compared with conventional load models. The corresponding results reveal that the proposed model is very accurate and robust, presenting superior performance. More specifically, the major advantages of the proposed method compared to other conventional load models are:

- The proposed model adopts an adjustable input/output formulation. Therefore, it can simulate accurately complex load dynamics, using variable-order linear transfer functions, while the optimal order is automatically determined, based on the desired accuracy. On the other hand, all conventional load models have a predetermined structure, and thus may fail to capture adequately high-order dynamics.
- The parameters of the conventional load models are estimated using NLS optimization techniques. These techniques are highly affected by the initial conditions, leading to sub-optimal solutions. The parameters of the proposed model are independent on the initial guess, as the required voltage exponents are determined using simple algebraic equations, while the required poles and residues are estimated using the VF technique.
- The proposed model is very robust, considering the loading conditions, the level of voltage disturbance and the composition of the load, providing always very accurate results. The proposed methodology also leads to model parameters which are very robust considering the noisy conditions.
- The iterative procedure, used to determine the minimum required model order, is numerically efficient and stable, converging quickly with small execution times.
- Finally, the proposed extension to allow multi-signal analysis improves the applicability of the methodology and enhances the robustness of the derived dynamic models.

Therefore, the proposed model can be considered as a new reliable tool for power system load modeling and identification.

References

[1] "Standard load models for power flow and dynamic performance simulation," *IEEE Trans. on Power Syst.*, vol. 10, no. 3, pp. 1302–1313, Aug 1995.

[2] "Load representation for dynamic performance analysis of power systems," *IEEE Trans. on Power Syst.*, vol. 8, no. 2, pp. 472–482, May 1993.

[3] J. V. Milanovic, K. Yamashita, S. M. Villanueva, S. Z. Djokic, and L. M. Korunovic, "International industry practice on power system load modeling," *IEEE Trans. Power Syst.*, vol. 28, no. 3, pp. 3038–3046, Aug 2013.

[4] H. Bai, P. Zhang, and V. Ajjarapu, "A novel parameter identification approach via hybrid learning for aggregate load modeling," *IEEE Trans. Power Syst.*, vol. 24, no. 3, pp. 1145–1154, Aug 2009.

[5] A. Ellis, D. Kosterev, and A. Meklin, "Dynamic load models: Where are we?" in *2005/2006 IEEE/PES Trans. and Distr. Conf. and Exh.*, May 2006, pp. 1320–1324.

[6] V. Knyazkin, C. A. Canizares, and L. H. Soder, "On the parameter estimation and modeling of aggregate power system loads," *IEEE Trans. Power Syst.*, vol. 19, no. 2, pp. 1023–1031, May 2004.

[7] H. Renmu, M. Jin, and D. J. Hill, "Composite load modeling via measurement approach," *IEEE Trans. Power Syst.*, vol. 21, no. 2, pp. 663–672, May 2006.

[8] P. Kundur, *Power System Stability And Control*. New York: McGraw-Hill, 1994.

[9] P. Jazayeri, W. Rosehart, and D. T. Westwick, "A multistage algorithm for identification of nonlinear aggregate power system loads," *IEEE Trans. Power Syst.*, vol. 22, no. 3, pp. 1072–1079, Aug 2007.

[10] P. Regulski, D. S. Vilchis-Rodriguez, S. Djurovic, and V. Terzija, "Estimation of composite load model parameters using an improved particle swarm optimization method," *IEEE Trans. Power Del.*, vol. 30, no. 2, pp. 553–560, April 2015.

[11] D. Karlsson and D. J. Hill, "Modelling and identification of nonlinear dynamic loads in power systems," *IEEE Trans. Power Syst.*, vol. 9, no. 1, pp. 157–166, Feb 1994.

[12] K. Zhang, H. Zhu, and S. Guo, "Dependency analysis and improved parameter estimation for dynamic composite load modeling," *IEEE Trans. on Power Syst.*, 2016.

[13] J. A. de Kock, F. S. van der Merwe, and H. J. Vermeulen, "Induction motor parameter estimation through an output error technique," *IEEE Trans. on Energy Convers.*, vol. 9, no. 1, pp. 69–76, Mar 1994.

[14] B.-K. Choi, H.-D. Chiang, Y. Li, H. Li, Y.-T. Chen, D.-H. Huang, and M. G. Lauby, "Measurement-based dynamic load models: derivation, comparison, and validation," *IEEE Trans. Power Syst.*, vol. 21, no. 3, pp. 1276–1283, Aug 2006.

[15] P. Ju, E. Handschin, and D. Karlsson, "Nonlinear dynamic load modelling: model and parameter estimation," *IEEE Trans. Power Syst.*, vol. 11, no. 4, pp. 1689–1697, Nov 1996.

[16] A. Rouhani and A. Abur, "Real-time dynamic parameter estimation for an exponential dynamic load model," *IEEE Trans. on Smart Grid*, vol. 7, no. 3, pp. 1530–1536, May 2016.

[17] A. Miranian and K. Rouzbehi, "Nonlinear power system load identification using local model networks," *IEEE Trans. Power Syst.*, vol. 28, no. 3, pp. 2872–2881, Aug 2013.

[18] T. Hiyama, M. Tokieda, W. Hubbi, and H. Andou, "Artificial neural network based dynamic load modeling," *IEEE Trans. Power Syst.*, vol. 12, no. 4, pp. 1576–1583, Nov 1997.

[19] J. Y. Wen, L. Jiang, Q. H. Wu, and S. J. Cheng, "Power system load modeling by learning based on system measurements," *IEEE Trans. Power Del.*, vol. 18, no. 2, pp. 364–371, April 2003.

[20] C. H. Lu, "Wavelet fuzzy neural networks for identification and predictive control of dynamic systems," *IEEE Trans. Ind. Electr.*, vol. 58, no. 7, pp. 3046–3058, July 2011.

[21] I. F. Visconti, D. A. Lima, J. M. C. d. S. Costa, and N. R. d. B. C. Sobrinho, "Measurement-based load modeling using transfer functions for dynamic simulations," *IEEE Trans. Power Syst.*, vol. 29, no. 1, pp. 111–120, Jan 2014.

[22] D. J. Hill and I. A. Hiskens, "Dynamic analysis of voltage collapse in power systems," in *Decision and Control, 1992., Proceedings of the 31st IEEE Conference on*, 1992, pp. 2904–2909 vol. 3.

[23] NEPLAN Help, NEPLAN Version 5.5.5.R1, Copyright (C) 1988-2010.

[24] C. J. Lin, A. Y. T. Chen, C. Y. Chiou, C. H. Huang, H. D. Chiang, J. C. Wang, and L. Fekih-Ahmed, "Dynamic load models in power systems using the measurement approach," *IEEE Trans. Power Syst.*, vol. 8, no. 1, pp. 309–315, Feb 1993.

[25] B. K. Choi and H. D. Chiang, "Multiple solutions and plateau phenomenon in measurement-based load model development: Issues and suggestions," *IEEE Trans. on Power Syst.*, vol. 24, no. 2, pp. 824–831, May 2009.

[26] B. Gustavsen and A. Semlyen, "Rational approximation of frequency domain responses by vector fitting," *IEEE Trans. Power Del.*, vol. 14, no. 3, pp. 1052–1061, Jul 1999.

[27] A. Beygi and A. Dounavis, "An instrumental variable vector-fitting approach for noisy frequency responses," *IEEE Trans. on Microwave Theory and Techniques*, vol. 60, no. 9, pp. 2702–2712, Sept 2012.

[28] B. Gustavsen, "Improving the pole relocating properties of vector fitting," *IEEE Trans. Power Del.*, vol. 21, no. 3, pp. 1587–1592, July 2006.

[29] F. Ferranti, Y. Rolain, L. Knockaert, and T. Dhaene, "Variance weighted vector fitting for noisy frequency responses," *IEEE Microwave and Wireless Components Letters*, vol. 20, no. 4, pp. 187–189, April 2010.

[30] J. V. Milanovic and S. M. Zali, "Validation of equivalent dynamic model of active distribution network cell," *IEEE Trans. Power Syst.*, vol. 28, no. 3, pp. 2101–2110, Aug 2013.

[31] S. M. Zali and J. V. Milanovic, "Generic model of active distribution network for large power system stability studies," *IEEE Trans. Power Syst.*, vol. 28, no. 3, pp. 3126–3133, Aug 2013.

[32] D. Kahaner, C. Moler, and S. Nash, *Numerical Methods and Software*. Englewood Cliffs, NJ: Prentice Hall, 1989.

[33] P. Moreno and A. Ramirez, "Implementation of the numerical laplace transform: A review," *IEEE Trans. Power Del.*, vol. 23, no. 4, pp. 2599–2609, Oct 2008.

[34] T. A. Papadopoulos, A. I. Chrysochos, E. O. Kontis, P. N. Papadopoulos, and G. K. Papagiannis, "Measurement-based hybrid approach for ringdown analysis of power systems," *IEEE Trans. on Power Syst.*, vol. 31, no. 6, pp. 4435–4446, Nov 2016.

[35] D. P. Stojanovic, L. M. Korunovic, and J. Milanovic, "Dynamic load modelling based on measurements in medium voltage distribution network," *Elect. Power Syst. Res.*, vol. 78, no. 2, pp. 228 – 238, Feb 2008.

[36] Cigre Report, Working Group C4.605. Modelling and aggregation of loads in flexible power networks, Feb. 2014.

[37] I. A. Hiskens, "Nonlinear dynamic model evaluation from disturbance measurements," *IEEE Trans. on Power Syst.*, vol. 16, no. 4, pp. 702–710, Nov 2001.

[38] Ugray, Zsolt, L. Lasdon, J. C. Plummer, F. Glover, K. James, and R. Martí, "Scatter search and local nlp solvers: A multistart framework for global optimization," *INFORMS Jour. on Computing*, vol. 19, no. 3, pp. 328–340, Jul. 2007.

[39] F. Glover, "A template for scatter search and path relinking," in *Artificial Evolution*. Springer, 1998, pp. 13–54.

[40] S. Grivet-Talocia and B. Gustavsen, *Passive Macromodeling: Theory and applications*. Wiley, 2016.

[41] J. Ning, X. Pan, and V. Venkatasubramanian, "Oscillation modal analysis from ambient synchrophasor data using distributed frequency domain optimization," *IEEE Trans. on Power Syst.*, vol. 28, no. 2, pp. 1960–1968, May 2013.

[42] J. Ning, S. A. N. Sarmadi, and V. Venkatasubramanian, "Two-level ambient oscillation modal estimation from synchrophasor measurements," *IEEE Trans. on Power Syst.*, vol. 30, no. 6, pp. 2913–2922, Nov 2015.

[43] R. L. Allen and D. Mills, *Signal Analysis: Time, Frequency, Scale, and Structure*. Wiley, 2004.

[44] S. A. Arefifar and W. Xu, "Online tracking of voltage-dependent load parameters using ultc created disturbances," *IEEE Trans. Power Syst.*, vol. 28, no. 1, pp. 130–139, Feb 2013.

[45] W. Xu, E. Vaahedi, Y. Mansour, and J. Tamby, "Voltage stability load parameter determination from field tests on bc hydro's system," *IEEE Trans. Power Syst.*, vol. 12, no. 3, pp. 1290–1297, Aug 1997.

[46] Measurement-Based Load Modeling. EPRI, Palo Alto. CA: 2006. 1014402.

Eleftherios O. Kontis (S'15) received the Dipl. Eng. Degree from the School of Electrical and Computer Engineering at the Aristotle University of Thessaloniki, in 2013. Since 2014, he has been Ph.D. student at the same university. His research interests are in the field of power system modeling, simulation and dynamic analysis of distribution networks and smart grids.

Theofilos A. Papadopoulos (S'01-M'09) received the Dipl. Eng. and Ph.D. degrees from the School of Electrical and Computer Engineering at the Aristotle University of Thessaloniki, Greece, in 2003 and 2008, respectively. He is currently Asst. Professor at the Power Systems Laboratory of the Department of Electrical and Computer Engineering of the Democritus University of Thrace, Greece. His special interests are power systems modeling, PLC and computation of electromagnetic transients. He received the Basil Papadias Award at the IEEE PowerTech 07 Conference.

Andreas I. Chrysochos (S'08-M'16) received the Dipl. Eng. and Ph.D. degrees from the School of Electrical and Computer Engineering at the Aristotle University of Thessaloniki, Greece, in 2009 and 2015 respectively. He is currently Post-Doc researcher at the Department of Electrical and Computer Engineering in Democritus University of Thrace as well as R&D Senior Engineer in Cablel® Hellenic Cables S.A., Viohalco Group. His special interests are power systems modeling, computation of electromagnetic transients, and PLC. He has been a scholar of the Alexander S. Onassis Public Benefit Foundation (2012-2015, 2016-2017).

Grigoris K. Papagiannis (S'79-M'88-SM'09) received his Dipl. Eng. Degree and the Ph.D. degree from the School of Electrical and Computer Engineering at the Aristotle University of Thessaloniki, in 1979 and 1998, respectively. He is currently Professor at the Power Systems Laboratory of the School of Electrical and Computer Engineering of the Aristotle University of Thessaloniki, Greece. His special interests are power systems modelling, computation of electromagnetic transients, distributed generation and PLC.